ACS OMEGA

http://pubs.acs.org/journal/acsodf

Article

Significant Improvement of Adsorption for Phosphate Removal by Lanthanum-Loaded Biochar

Sainan Xia, Shengrong Liang, Yixue Qin, Weijie Chen, Bin Xue, Bingbing Zhang,* and Guomin Xu*

Cite This: *ACS Omega* 2023, 8, 24853−24864

Read Online

ACCESS | Metrics & More | Article Recommendations

ABSTRACT: Due to eutrophication, removing phosphate ions from wastewater has received a lot of attention. In order to improve the phosphorus adsorption capacity of the material, this study used biomass pyrolysis to create a series of biochars modified with metal chloride ions. In accordance with adsorption tests, lanthanum-loaded biochar (LCBC) had a significant phosphorus adsorption capacity of approximately 666.67 mg/g, which was 30 times greater than that of pristine biochar. Adsorption kinetic analysis revealed that the LCBC's adsorption process could be fitted to the pseudo-secondary kinetic equation, indicating that chemical processes were primarily responsible for controlling the adsorption process. Zeta potential, Fourier transform infrared spectroscopy, and X-ray photoelectron spectroscopy analysis showed that the main adsorption mechanism of LCBC for phosphate removal was electrostatic attraction of protonated H+ with negatively charged mono-hydrogen phosphate and dihydrogen phosphate ions and complexation reaction of the C═O on the carboxyl group and P═O on the phosphate group with the oxygen on the phosphate group and hydroxyl group. According to regeneration performance results, LCBC performed relatively better than as-prepared adsorbents, and the phosphate removal rate was approximately 75.1% after the fifth regeneration cycle. The study provided a potential approach for creating and preparing an adsorbent with high adsorption for phosphate removal.

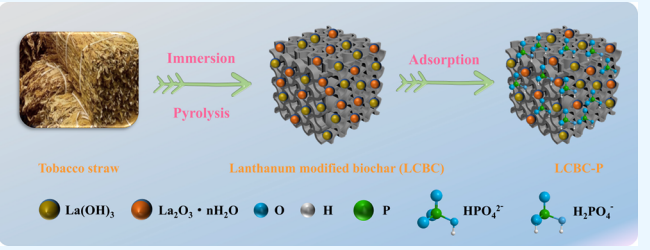

1. INTRODUCTION

In recent years, eutrophication pollution caused by wastewater containing phosphorus has gained attention among scientific communities.[1,2] Numerous techniques have been used to remove phosphorus from wastewater,[3] including biological methods,[4,5] chemical precipitation,[6,7] electrolysis,[8,9] adsorption,[10−12] and so on. Among them, biochar adsorption[13] has received a lot of attention due to its environmental and economic benefits.[14] Generally, biochar has a negative surface charge that limits its binding affinity to phosphate anions. Moreover, it has been found that the adsorption capacity of biochar could be further improved by modifying its morphological structure.[15,16] In fact, one of the typical problems that researchers focused was adjusting the microstructure of adsorbents to increase the adsorption capacity.

Over the past years, numerous attempts have been made to modify adsorbents to enhance their phosphorus adsorption capacity, and metal ion-loaded modification has been widely studied.[17,18] The capacity of the modified adsorbents to adsorb phosphorus was significantly affected by the types of metal ions. Li et al.[19] prepared a series of Fe-modified biochar by pyrolyzing the corn straw impregnated with $FeCl_3$ solution at various temperatures. The maximum phosphorus adsorption capacity of the adsorbent was discovered to be 26.14 mg/g, which was up 253.2 percent from pristine biochar. Koh et al.[20] reported a hydrothermally synthesized lanthanum carbonate (LC) nanorod for removal of phosphate. They discovered that the maximum adsorption capacities of 312.5 and 303.03 mg/g were found at pH 5 and 7, respectively. According to Deng et al.,[21] biochar modified by various metal ions displayed various surface morphological structures and phosphorus adsorption properties. The theoretical maximum phosphate adsorption capacities of 20% Mg-BC and 20% Al-BC are 56.12 and 44.79 mg/g, respectively. Wu et al.[22] investigated the effects of lanthanum carbonate (LC) and lanthanum hydroxide (LH) treatments on phosphorus. Results showed that LC outperformed LH for phosphate adsorption in pure aqueous solution at pH 5−7, but the latter possessed higher adsorption ability for phosphate in pure aqueous solution at pH 8−11 than the former. Additionally, the adsorption process and corresponding selectivity of the composite for phosphorus are both impacted by the type of metal ions on the biochar. In spite of the two materials' similar maximum adsorption capacities, Huang et al.[23] found that lanthanum hydroxide/

Received: February 7, 2023
Accepted: June 26, 2023
Published: July 10, 2023

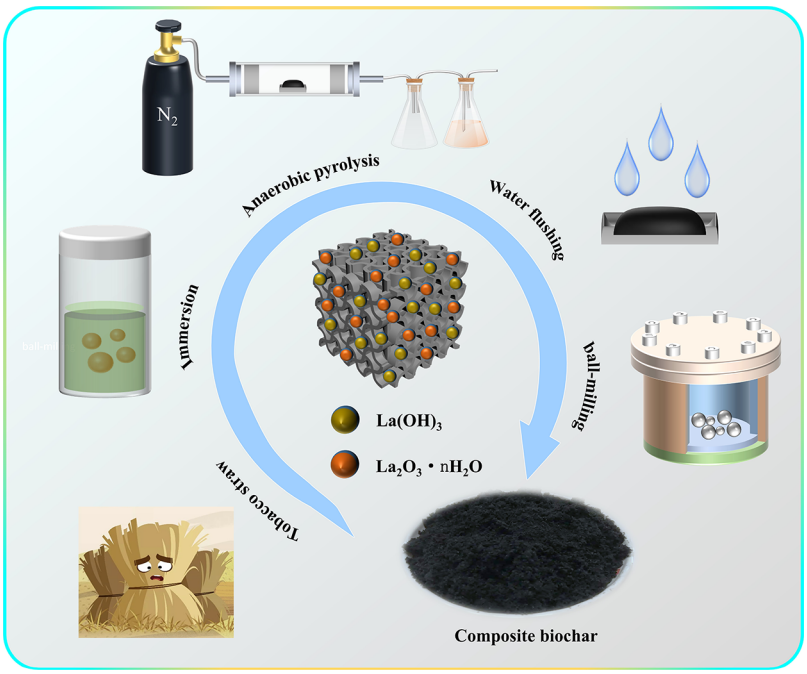

Figure 1. Scheme of the LCBC preparation procedure.

biochar had a higher selectivity for phosphorus (90−100%) than lanthanum carbonate/biochar (73−99%). In addition, composite metal ion-loaded modification also affects the adsorption properties of adsorbents. Shi et al.[24] prepared a novel La-incorporated nanostructured ternary (hydr)oxide adsorbent (MALZ). The results of scanning electron microscopy (SEM) and X-ray diffraction (XRD) indicated that MALZ presented an amorphous surface with Mg, Al, and La homogeneously dispersed on the outer region of zeolite. The maximum adsorption capacity of MALZ was determined at 80.8 mg P/g at pH 6.6. Li et al.[25] prepared a highly efficient phosphorus adsorbent of ZnAl-LDO-BC by ethanol intensification and the banana straw co-precipitation method. At the initial condition of 500 mg/L phosphorus at 45 °C, ZnAl-LDO-BC had a theoretical maximum adsorption capacity of 111.11 mg/g. From the above studies, it is concluded that phosphate adsorption performance of the metal ion-modified biochar was determined by the specific modifiers, composition, and preparation processing. Therefore, there is still a need for numerous additional studies.

In this study, tobacco sticks impregnated with lanthanum chloride heptahydrate aqueous solution were pyrolyzed to create lanthanum-modified biochar. For comparison with lanthanum-modified biochar, tobacco sticks were also modified using aqueous ferric chloride and zinc chloride hexahydrate. We conducted a thorough analysis of the as-prepared biochar's adsorption behavior and performance, and the mechanism of lanthanum-loaded biochar's phosphate adsorption was also discussed. In addition, the regeneration performance of the as-prepared biochar was evaluated as well. It is believed that this study provides a new approach for modifying biochar with high adsorption capacity.

2. MATERIALS AND METHODS

2.1. Materials. Tobacco sticks were collected from around Guiyang. Chemical agents for modified tobacco sticks included ferric chloride hexahydrate ($FeCl_3{\cdot}6H_2O$), zinc chloride ($ZnCl_2$), and lanthanum chloride heptahydrate ($LaCl_3{\cdot}7H_2O$) which were all analytical reagents (AR), and all were purchased from Damao Company, Shanghai Yien Chemical Technology Co., Ltd., and Tianjin Upu Chemical Reagent Co. Ltd., respectively. Potassium dihydrogen phosphate (KH_2PO_4) powder was dissolved in deionized water to create various phosphate concentrations. The deionized water was prepared by the laboratory system. In this study, all the experiments were performed in triplicate and data were presented as mean ± standard deviation (SD: standard deviation, n = 3).

2.2. Preparation and Modification. To prepare the virgin biochar, the tobacco sticks were pyrolyzed at 400 °C and held for 2 h with nitrogen flow. The biochar (BC) was repeatedly rinsed with deionized water. Finally, it was dried in an oven. Furthermore, biochar needed to be modified further in order to remove phosphorus effectively.

Biochar modified by lanthanum was generated through an impregnation and pyrolysis process (Figure 1). In a nutshell, the powdered tobacco sticks were immersed in a $LaCl_3{\cdot}7H_2O$ solution at a mass concentration of 60% for 24 h. Samples were then dried by being heated at 120 °C for 12 h. The impregnated samples were pyrolyzed at 500 °C and retained for 1 h under nitrogen flow to prepare the biochar (LCBC). Deionized water was used to repeatedly rinse the biochar. It was then dried in an oven. The corresponding ferric-modified biochar and zinc-modified biochar were designated FCBC and ZCBC, respectively.

2.3. Adsorbent Characterization. The crystalline structure of the material was measured using XPert PRO MPD type XRD. SEM and energy-dispersive spectrometry were used to examine the composite's surface morphology and chemical composition. An infrared spectrometer with Fourier transform was used to measure the functional groups of biochar (FTIR). Using a Malvern Zetasizer Nano ZS90 zeta potential analyzer, the surface charge of the biochar before and after modification was determined. The elemental composition of the material was determined using a Thermo Scientific K-Alpha X-ray

https://doi.org/10.1021/acsomega.3c00788
ACS Omega 2023, 8, 24853−24864

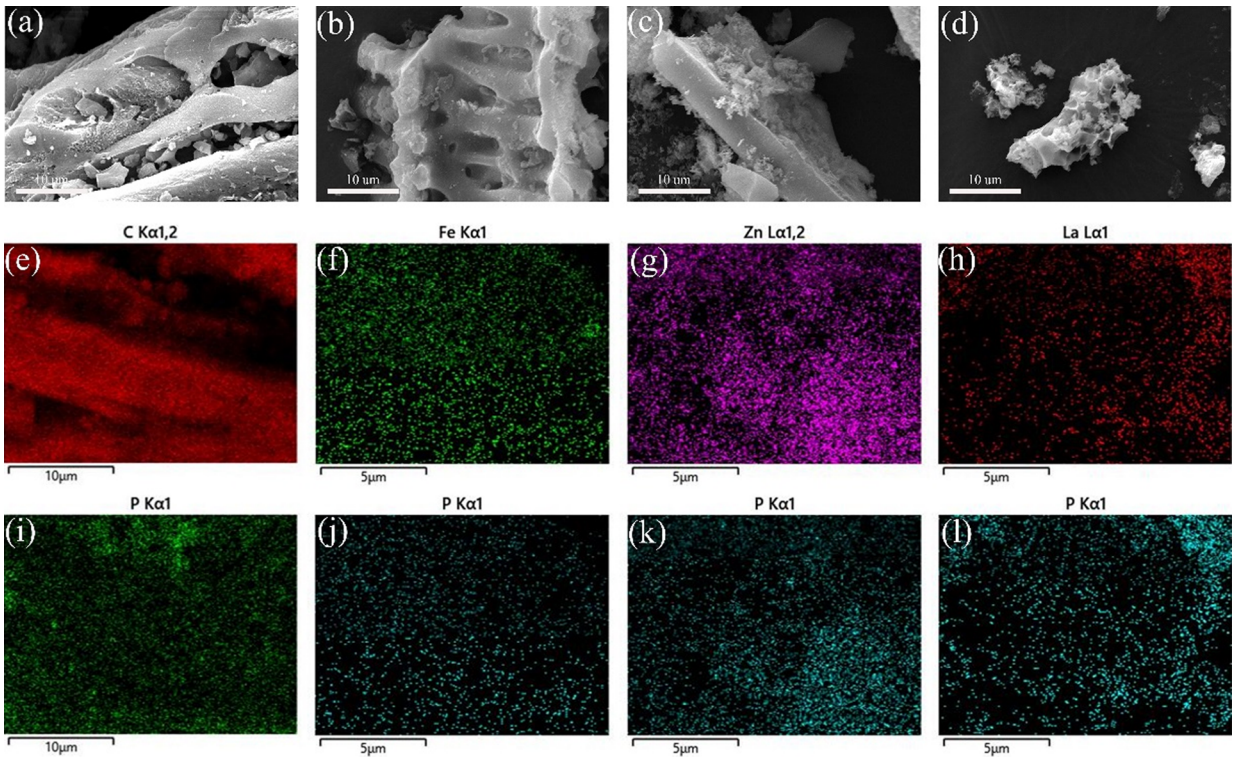

Figure 2. SEM images of (a) BC, (b) FCBC, (c) ZCBC, and (d) LCBC; elemental mapping images of (e, i) BC-P, (f, j) FCBC-P, (g, k) ZCBC-P, and (h, l) LCBC-P.

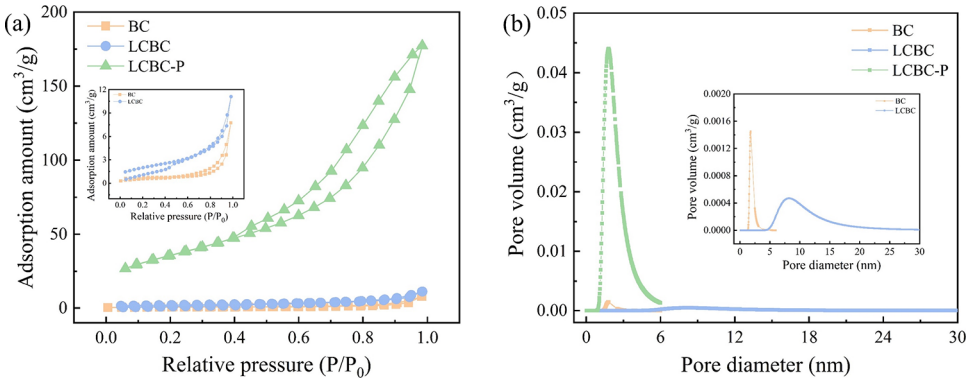

Figure 3. (a) N_2 adsorption and desorption curves and (b) pore size distribution of BC, LCBC, and LCBC-P.

photoelectron spectroscopy (XPS). The multipoint N_2 Brunauer−Emmett−Teller (BET) method was used to measure the biochar's specific surface area and pore size distribution at 77 K. To measure the phosphate concentration, a 952 N UV−vis spectrophotometer (Shanghai Yidian Analytical Instruments Co., Ltd.) was used. The material mass was measured using an electronic balance (OHAUS Instruments Co., Ltd.).

2.4. Adsorption Experiments. A series of batch adsorption experiments were performed in a shaker oscillated at 200 rpm and 30 ± 0.5 °C to measure the adsorption and removal of the biochar for phosphorus as it was prepared. After the adsorption reaction, the solutions were filtered by a 0.45 μm microporous membrane filter. In acidic medium, orthophosphate reacts with ammonium molybdate to form phosphomolybdenum heteropoly acid in the presence of antimony salt, which is immediately reduced by ascorbic acid to form a blue complex (phosphomolybdenum blue). The color depth is proportional to the total phosphorus content, which can be measured colorimetrically at 700 nm. A UV−visible spectrophotometer operating at a wavelength of 700 nm was used to measure the equilibrium concentration of phosphorus ions in the solution. The phosphorus removal rate was calculated by eq 1:

$$R = \frac{C_0 - C_e}{C_0} \times 100\% \quad (1)$$

where R (%) is the phosphorus removal rate, C_0 (mg/L) is the initial concentration of phosphorus ions before adsorption, and C_e (mg/L) is the equilibrium concentration of phosphorus ions in the solution.[2,26] In addition, the adsorption capacity q_e of phosphorus per material was calculated as:

$$q_e = V \times \frac{C_e - C_0}{M} \quad (2)$$

https://doi.org/10.1021/acsomega.3c00788
ACS Omega 2023, 8, 24853−24864

where q_e (mg/g) is the equilibrium adsorption capacity, V (L) is the volume of solution, and M (g) is the mass of adsorbent.[27−30]

3. RESULTS AND DISCUSSION

3.1. Characterization of Adsorbents. Figure 2 displays the elemental energy spectra of BC-P, FCBC-P, ZCBC-P, and LCBC-P as well as the SEM images of BC, FCBC, ZCBC, and LCBC. The morphology of biochar was primarily skeleton-shaped, as can be seen in Figure 2a−d, and each biochar particle was about 50 um in size. The BC had a relatively smooth and clean surface. However, there were some material lumps on the surfaces of FCBC, ZCBC, and LCBC. It can be argued that the metal loading on the biochar improves its ion exchange capacity and expands its surface area for adsorption sites.[19] The surface of ZCBC showed a floccule structure. It may have a larger specific surface area. The surface of LCBC had a honeycomb shape, which provided more active centers.[31] The modifier has been grafted onto the biochar in Figure 2f−h. Similarly, Figure 2i−l demonstrates that all four adsorbents adsorbed phosphorus. For FCBC-P, ZCBC-P, and LCBC-P, the amount of phosphorus adsorbed increased with the amount of metal elements loaded onto the biochar. It can be concluded that the distribution of metal on the biochar is consistent with that of phosphorus on the biochar for the three modified adsorbents.

The N_2 adsorption−desorption isotherms and pore size distributions of BC, LCBC, and LCBC-P are shown in Figure 3a,b. All three isotherms belong to type IV adsorption isotherms and the H_3 hysteresis loop exists, indicating the existence of slit pores in the material.[32] It can be found in Figure 3b that loaded lanthanum can increase the pore size of biochar. Table 1 displays the four materials' average pore size, pore volume, and specific surface area. The specific surface area of BC is 2.786 m^2/g, and the maximum can be 48.55 m^2/g after modification. Table 1 shows that the three modified adsorbents had greater specific surface areas and pore volumes than BC. This is due to the modified reagent's activation effect, which increases pore volume and increases the specific surface area of biochar. The ability of phosphorus to transfer from solution to adsorbent surface is improved by increasing the surface area of biochar,[19] which is beneficial for phosphorus adsorption. The presence of metal adsorption sites on the surface and in the pores of the three modified biochars and the filling of the inner microspores with the loaded particles could account for the slight increases in pore volume.[33] The specific surface area and total pore volume increase, while the pore size decreases after phosphorus adsorption by four adsorbents (Table 1). The reason may be that phosphorus was adsorbed on the surface of the adsorbent and the soluble substance in the volatile phosphorous solution, causing the surface to increase. This indicates that modification and adsorption of phosphorus have significant effects on the pore development of biochar.

Table 1. Surface and Structure Characteristics of Four Adsorbents before and after Adsorption

sample	surface area S_{BET} ($m^2\ g^{-1}$)	pore volume V_p ($cm^3\ g^{-1}$)	pore diameter D_{BJH} (nm)
BC	2.786	0.005	7.69
FCBC	19.30	0.074	153.56
ZCBC	48.55	0.021	99.52
LCBC	7.14	0.017	96.16
BC-P	13.93	0.023	6.54
FCBC-P	56.17	0.119	85.47
ZCBC-P	161.36	0.110	2.73
LCBC-P	130.04	0.274	8.43

According to Figure 4a, the complexation reactions that can take place on the surface of the biochar are based on the peaks at wavenumbers 3560, 1617, and 1435 cm^{-1} that are attributed to the telescopic vibrations of the −OH, C═O, and C═C.[34] The narrow scan peaks of the C1s peaks are shown in Figure 4b: Three singlets from the C1s peak show C═C, C−OH, and COOH. This implies that the functional group content of all four adsorbents is high. In Figure 4a, 465 cm^{-1} is the result of Fe−OH stretching vibrations.[19] This phenomenon proves that iron was successfully loaded on the modified biochar. In Figure 4a, 713 cm^{-1} is the peak of Zn−O, indicating that the biochar is loaded with zinc. LCBC at 720 and 552 cm^{-1} corresponds to the peaks of La−OH and O−P−O,[35] respectively. Another indication that La was successfully loaded onto biochar is the characteristic peak of LCBC at 513 cm^{-1}, which is associated with the vibration of the La−O bond.[36]

Figure 5 shows the XRD patterns of BC, FCBC, ZCBC, and LCBC. It is seen that amorphous carbon was detected in both BC and FCBC,[19] and a similar pattern of BC and FCBC indicated that there was mainly an amorphous structure existing in FCBC.[27] On the other hand, ZCBC showed diffraction peaks at 29.26 (002), 33.11 (002), 37.58 (101), 51.53 (013), and 58.27 (021), indicating that ZnO was primarily formed in ZCBC.[37] While $La(OH)_3$ was produced in LCBC primarily at 28.108, 39.565, and 47.138°,[31] the

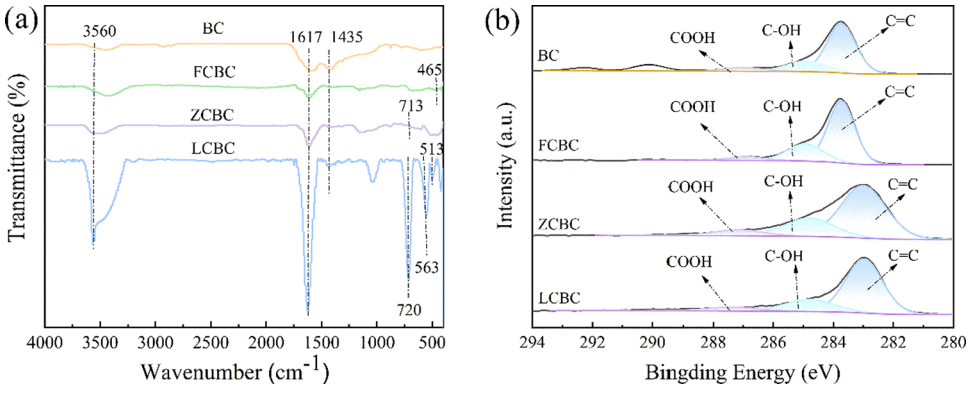

Figure 4. (a) FT-IR patterns and (b) XPS C 1s spectra of four adsorbents.

https://doi.org/10.1021/acsomega.3c00788
ACS Omega 2023, 8, 24853−24864

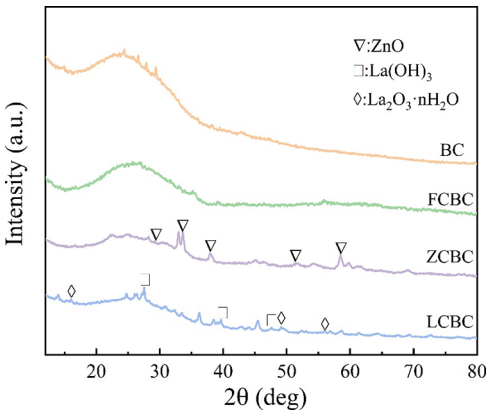

Figure 5. XRD patterns of (a) BC, (b) FCBC, (c) ZCBC, and (d) LCBC.

diffraction peaks at 15.7° (100), 48.6° (211), and 55.3° (112) demonstrated that hydrated lanthanum oxides were formed in LCBC.[38]

3.2. Adsorption of the As-Prepared Biochar for Phosphorus Removal Performance. *3.2.1. Effect of Contact Time.* This section added 2 g/L each of BC, FCBC, ZCBC, and LCBC to a phosphate solution with a concentration of 600 mg/L. In a reciprocating water bath thermostat oscillator set to 30 °C, the solution was then vibrated at 200 rpm. We examined the residual phosphate content over time periods of 3, 10, 30, 60, 120, 180, 240, 300, 420, 540, 1200, and 1440 min.

According to Figure 6a, the adsorption capacity of the different biochar all increased with increasing adsorption time, and the adsorption efficiency exhibited a tendency to increase initially before leveling off over time. The removal rate of phosphorus by four adsorbents increased first and then remained constant with the extension of time. The adsorption equilibrium of the four adsorbents was reached in 120 min. The adsorption process can be divided into two stages: stage one is the rapid adsorption stage. Phosphate was easy to combine with the adsorbent in the presorption stage because it had a large number of adsorption sites. The second stage is known as the slow adsorption stage, during which the adsorption sites gradually decrease and slowly reach saturation. Overall, the adsorption capacity and removal rate of LCBC were higher than those of the other three adsorbents at any time point.

3.2.2. Effect of Initial Concentration. In this section, 2 g/L BC, FCBC, ZCBC, and LCBC were respectively added into phosphate solution with a concentration of 10, 50, 100, 200, 400, and 600 mg/L. A reciprocating water bath thermostat oscillator was used to vibrate the solution for 24 h at 200 rpm.

The phosphorous adsorption capacity and removal rate of BC, FCBC, ZCBC, and LCBC are displayed in Figure 6b. The FCBC, ZCBC, and LCBC exhibit excellent adsorption effects at low concentrations, and the four adsorbents effectively recover phosphate from water even at a relatively low phosphorus concentration. The adsorption capacity of the four biochars gradually increases as the initial phosphorus concentration rises, and the removal rate of phosphorus generally shows a downward trend. In a word, the adsorption capacity and removal rate of BC were 30.29 mg/g and 10.1% at

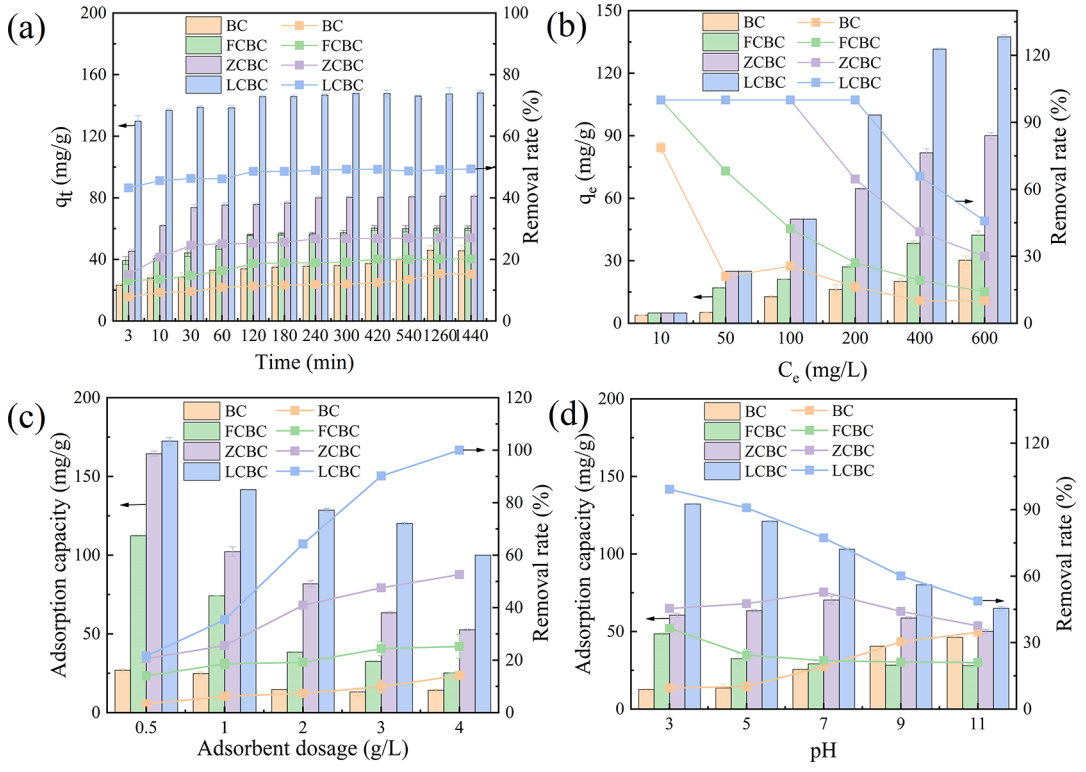

Figure 6. Adsorption capacity and removal rate on four adsorbents of (a) time courses (temperature, 30 °C; in initial phosphorus concentration, 600 mg/L; dosage, 2 g/L), (b) initial phosphorus concentration (temperature, 30 °C; dosage, 2 g/L; contact time,24 h), (c) adsorbent dosage (temperature, 30 °C; in initial phosphorus concentration, 400 mg/L; contact time, 24 h), and (d) solution pH (temperature, 30 °C; in initial phosphorus concentration, 400 mg/L; dosage, 3 g/L; contact time, 24 h).

https://doi.org/10.1021/acsomega.3c00788
ACS Omega 2023, 8, 24853−24864

600 mg/L, respectively. LCBC had the highest removal rate and adsorption capacity when compared to other adsorbents. The adsorption capacity and removal rate of LCBC were 137.44 mg/g and 45.8% at 600 mg/L, respectively.

3.2.3. Effect of Adsorbent Dosage. In this section, phosphate solution with a concentration of 400 mg/L and known masses of BC, FCBC, ZCBC, and LCBC (0.5, 1, 2, 3, and 4 g/L) was added, respectively. The solution was then vibrated at 200 rpm for 24 h at 30 °C in a reciprocating water bath thermostat oscillator.

According to Figure 6c, at a given concentration, the removal rate increases and the adsorption capacity of the four types of biochar decreases with increasing dosage. It is clear that the modified biochar was more effective at adsorbing and removing phosphorus than the BC, regardless of the adsorbent's concentration. When the adsorbent concentration was 4 g/L, the removal rate of phosphorus was only 14.2% for the BC, 25.22% for the FCBC, and 52.62 and 100% for the ZCBC and LCBC, respectively. The result indicates that LCBC was an efficient phosphorus removal material to efficiently remove phosphorus from sewage.

3.2.4. Effect of pH. In this section, the pH of the solution adjusted by 0.1 mol/L NaOH and HCl was 3.0, 5.0, 7.0, 9.0, and 11.0, respectively. Phosphate solution with a concentration of 400 mg/L received additions of 3 g/L each of BC, FCBC, ZCBC, and LCBC. Then the solution was vibrated at 200 rpm in a reciprocating water bath thermostat oscillator at 30 °C for 24 h.

The effect of solution pH on the adsorption capacity and removal rate is displayed in Figure 6d. BC had a minimum adsorption capacity of 3.85 mg/g at pH 3, while LCBC had a maximum adsorption capacity of 132.22 mg/g. The smallest removal rate of BC was 23.09% at pH 3. LCBC had the highest removal efficiency at this time, at 99.16%. With an increase in pH, the removal rates of FCBC and LCBC differ significantly, with the LCBC experiencing a 50.4% decrease. The adsorption removal rate of BC gradually increased as the pH of the solution rise, while the adsorption removal rates of FCBC and LCBC gradually decreased. When pH = 7, the adsorption capacity of ZCBC reaches the maximum. Phosphates in solution are mainly $H_2PO_4^-$ ions, which have a greater affinity for zinc than other pH values.[37] However, in real life, phosphorus in water is acidic. Theoretically, when the pH of solution is under 2.1, the main form of phosphorus in solution is H_3PO_4. When pH is 2.1−7.20, the dominant form of P is $H_2PO_4^-$. At pH 7.2−12.3, the main form of P changes to HPO_4^{2-}, and at pH higher than 12.3, the main form of P changes to PO_4^{3-} (Figure 7). Therefore, LCBC can be used in the industrial wastewater of phosphorus chemical production.

3.3. Adsorption Kinetics. For the phosphorus adsorption on biochar, pseudo-first-order (eq 3) and pseudo-second-order (eq 4) kinetic models were used, respectively.[19,27]

$$q_t = q_e(1 - e^{-tK_1}) \quad (3)$$

$$q_t = \frac{tK_2q_e^2}{1 + tK_2q_e} \quad (4)$$

where q_t (mg/g) denotes the adsorbed amount of phosphate at time t, q_e is the equilibrium adsorption capacity (mg/g), t is the adsorption time, min, and K is the kinetic constant.

Their kinetic fitting curves are displayed in Figure 8 along with a list of the kinetic parameters in Table 2. The

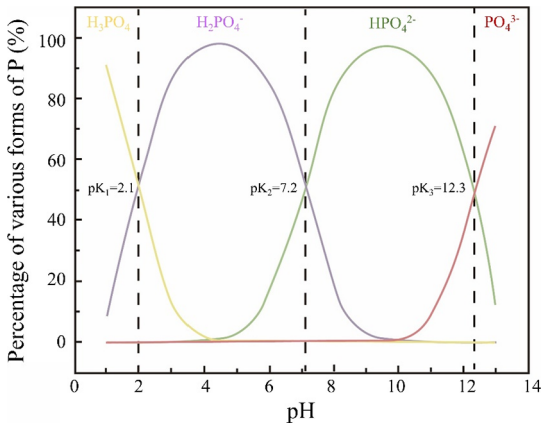

Figure 7. Percentage of various forms of P.

experimental data fit with the pseudo-second-order kinetic model more closely than the pseudo-first-order kinetic model ($R_2^2 > R_1^2$), indicating that chemisorption between phosphate and the active sites of the absorbent may be the primary process of phosphate adsorption.[31,35,39] The pseudo-second-order kinetic model predicted that the adsorbent and phosphorus shared electrons. Additionally, the pseudo-second-order model's results for the equilibrium adsorption capacities of BC, FCBC, ZCBC, and LCBC were 46.51 mg P/g, 60.61 , 89.29, and 147.06 mg P/g, respectively, and the results were consistent with the experiments. The pseudo-second-order model revealed that the K_2 values for BC and LCBC were 0.0007 and 0.0033 g/(min mg), respectively, and that LCBC adsorbs phosphorus at the fastest rate.

In order to further describe the adsorption process on biochar, the intraparticle diffusion (eq 5) was also explored.[40] If the fitted lines of intraparticle diffusion do not pass through the origin, then intraparticle diffusion is not the only diffusion mechanism.[2,35]

$$q_t = K_3t^{0.5} + C \quad (5)$$

where q_t (mg/g) denotes the adsorbed amount of phosphate at time t; K is the kinetic constant and C is a constant.

It can be inferred from Figure 8c that intraparticle diffusion controls the phosphate adsorption process on the modified biochar.[35,38] The adsorption process can be roughly divided into three stages: fast stage, slow stage, and equilibrium stage. Concentration differences and chemisorption caused by the functional groups of the biochar in the first adsorption stage were the driving forces.[32] The second linear segment had a slower slope, indicating that pore or void diffusion was the slow, rate-limiting process responsible for the adsorption process. The second stage does not pass through the origin, indicating that the adsorption process was controlled by other adsorption stages. In the third stage, the diffusion of phosphorus in the particles was further slowed down because the adsorption sites on the adsorbent surface were occupied. The results of the model fitting demonstrated that chemical adsorption, which was primarily accomplished through surface adsorption and particle internal diffusion, was the rate-limiting step of phosphorus adsorption in wastewater by four adsorbents. The adsorption rate was controlled by the adsorption reaction between the adsorption site on biochar and phosphate ions. In addition, the phosphorus adsorption

https://doi.org/10.1021/acsomega.3c00788
ACS Omega 2023, 8, 24853−24864

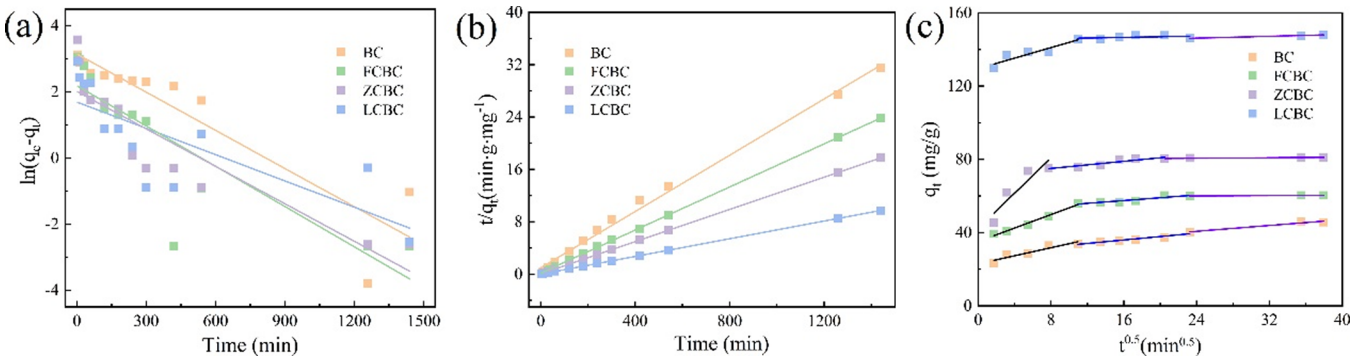

Figure 8. Linear fitting of kinetic models for phosphorus adsorption: (a) pseudo-first-order, (b) pseudo-second-order, and (c) intraparticle diffusion model fitting for phosphorus adsorption.

Table 2. Summary of the Parameters Obtained from the Pseudo-First Order Kinetic, the Pseudo-Second Order Kinetic, Intraparticle Diffusion Kinetic, and Freundlich and Langmuir Models for Adsorption of Phosphorus onto BC, FCBC, ZCBC, and LCBC[a]

model	parameters	BC	FCBC	ZCBC	LCBC
the pseudo-first-order kinetic	q_e^{cal} (mg/g)[b]	23.2	8.90	7.50	5.44
	K_1 (/min)	0.0038	0.0041	0.0038	0.0026
	R_1^2	0.8353	0.7491	0.8219	0.6108
the pseudo-second-order kinetic	q_e^{cal} (mg/g)[c]	46.51	60.61	89.29	147.06
	K_2 (g/(min mg))	0.0005	0.0016	0.0025	0.0033
	R_2^2	0.9948	0.9999	0.9999	0.9999
	q_e^{exp} (mg/g)[d]	45.98	60.33	81.80	147.4
intraparticle diffusion	K_{d1} (g/(mg/min$^{0.5}$))	1.101	1.889	4.810	1.435
	C_1	22.95	35.15	42.30	129.56
	R_3^2	0.8883	0.9863	0.8411	0.8512
	K_{d2} (g/(mg/min$^{0.5}$))	0.471	0.381	0.486	0.894
	C_2	28.43	51.41	71.16	145.17
	R_4^2	0.9171	0.8623	0.8367	0.1871
	K_{d3} (g/(mg/min$^{0.5}$))	0.395	0.024	0.035	0.127
	C_3	31.34	59.44	79.76	143.12
	R_5^2	0.9571	0.9758	0.8946	0.9689
Freundlich model	n	2.1119	1.9666	0.7046	1.1906
	K_F (mg/g)	1.343	1.852	1.333	0.876
	R_6^2	0.9869	0.9638	0.9357	0.9688
Langmuir model	q_{max} (mg/g)	22.12	40.49	212.77	666.67
	K_L (L/mg)	0.0215	0.0141	0.0024	0.0010
	R_7^2	0.9872	0.9972	0.9982	0.9996

[a] C_n (n = 1, 2, 3), C is the boundary layer thickness constant. [b] Calculated values for the pseudo-first-order kinetic. [c] Calculated values for the pseudo-second-order kinetic. [d] The experimental value.

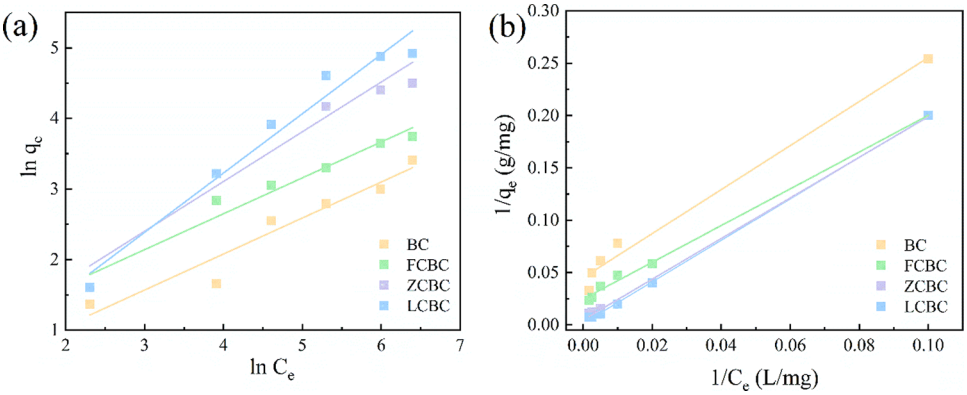

Figure 9. Linear fitting of (a) Freundlich and (b) Langmuir isotherm models for BC, FCBC, ZCBC, and LCBC.

https://doi.org/10.1021/acsomega.3c00788
ACS Omega 2023, 8, 24853−24864

capacities of four adsorbents ranged from high to low and were LCBC, ZCBC, FCBC, and BC, respectively.

3.4. Adsorption Isotherm. The type of PO_4^{3-} adsorption was investigated using the Freundlich (eq 6) and Langmuir (eq 7) adsorption isotherm models.[3,19,36]

$$q_e = K_F C_e^{1/n} \tag{6}$$

$$q_e = \frac{C_e q_m K_L}{1 + C_e K_L} \tag{7}$$

where q_e (mg/g) is the equilibrium adsorption capacity, K_F and n are Freundlich constants, C_e (mg/L) is the equilibrium concentration of phosphorus ions in the solution, q_m (mg/g) represents the maximum adsorption capacity of adsorbents, and K_L is the Langmuir constant.

The affinity between phosphate and biochar could be described by the dimensionless separation factor R_L (eq 8) from Langmuir parameters.[25,41]

$$R_L = \frac{1}{1 + C_0 K_L} \tag{8}$$

According to Figure 9 and Table 2, the R_7^2 calculated by the Langmuir model on the four adsorbents was higher than the R_6^2 calculated by the Freundlich model. It is suggested that the phosphate adsorption on BC, FCBC, ZCBC, and LCBC was caused by a monolayer homogenous adsorption process. Similarly, the Langmuir model estimated maximum adsorption capacities (q_m) for the BC, FCBC, ZCBC, and LCBC to be 22.12, 40.49, 212.77, and 666.67 mg/g (Table 2). LCBC's maximum adsorption capacity was significantly greater than the adsorption capacities of other three adsorbents and other La-loaded adsorbents previously reported in the literature (Table 3). The R_L of BC, FCBC, ZCBC, and LCBC was 0.824, 0.876, 0.977, and 0.990($0 < R_L < 1$), indicating that the phosphate adsorption on four samples was favorable.

Table 3. Comparison between LCBC and the Literature on the Adsorption Capacity of Lanthanum Adsorbents for Phosphate

adsorbents	lanthanum species	Q_{max} (mg P/g)	references
La-biochar		36.06	33
La−BC	LaOOH, $LaONO_3$ and $La(OH)_3$	46.37	36
La-coated sludge-based-biochar		93.91	35
La10-MC	$La(OH)_3$	101.16	42
La-TC	$La(OH)_3$	148.11	31
D-HLO	$La_2O_3{\cdot}nH_2O$	148.31	38
La-SSBC	$La(OH)_3$	312.55	43
LCBC	$La(OH)_3$ and $La_2O_3{\cdot}nH_2O$	666.67	this study

3.5. Evaluation of Regeneration Performance. A desorption experiment was conducted on PO_4^{3-}-loaded samples to ascertain the reusability of the tested adsorbents and the availability of adsorbed PO_4^{3-}. In this study, the eluents of BC, FCBC, ZCBC, and LCBC were 10% NaOH/5% NaCl. Five regeneration cycles of four different adsorbents were examined, and the changes in adsorption efficiency were calculated and analyzed. Each experiment was repeated three times.

As shown in Figure 10a, the removal rates of BC, FCBC, ZCBC, and LCBC were initially 14.5, 67.3, 100 and 100% respectively, but after the fifth regeneration cycles rates were decreased to 14.2, 23.1, 19.9, and 75.1% respectively. Because lanthanum has a higher phosphate affinity, it is obvious that LCBC demonstrated a better regeneration performance than other adsorbents. Furthermore, LCBC has more active sites reversed in the desorption process than other adsorbents.

3.6. Adsorption Mechanism. *3.6.1. Zeta Potential.* Figure 10b depicts the zeta potential of four adsorbents, which is a crucial marker of the stability of the dispersion system and influences the kind and amount of surface charge of biochar.[44] It can be seen from Figure 10b that the pH_{iep} of BC and LCBC were 2.98 and 9.60 respectively. When the pH is lower than pH_{iep}, the biochar surface becomes positively charged due to protonation and will combine with phosphate through electrostatic attraction. As the pH increases, the zeta potential became negative, which is not conducive to the adsorption of anions.[45] By electrostatic interaction, the surface protonation H^+ of LCBC adsorbs negatively charged mono- and dihydrogen phosphate ions in acidic conditions. As the pH of the solution increased, the increased OH^- concentration in the solution system increases the competition between it and phosphate, thus making phosphate adsorption less efficient. On the other hand, the surface of biochar has a greater negative charge when the pH level is higher. It will lead to enhance the electrostatic inhibition of phosphate, thus reduce the adsorption capacity of phosphorus.[31,32] Due to its higher pH_{iep}, LCBC has better adsorption performance than the other three adsorbents.

3.6.2. FTIR Analysis. Phosphorus was successfully adsorbed by the four adsorbents, as shown in Figure 10c, where the peak near 1053 cm^{-1} corresponds to the P−O stretching vibration of the PO_4^{3-} group.[46] Additionally, 619 cm^{-1} corresponds to the bending vibration of the O−P−O group,[35] indicating that the phosphate was chemically bonded to the surface of the material. The P−O stretching vibrations correspond to the 1013 cm^{-1} peaks in ZCBC-P. The result showed that ZCBC can successfully adsorb phosphorus.[25] In LCBC-P, the peaks of 540 cm^{-1} also corresponds to the bend vibration of O−P−O.[35] This suggests that the inner sphere complex was created during phosphorus adsorption.[32] One of the factors contributing to LCBC's high adsorption capacity is the fact that only LCBC has two O−P−O peaks which can be observed in Figure 10c.

3.6.3. XPS Study. The XPS spectra of BC, FCBC, ZCBC, and LCBC before and after phosphate adsorption are displayed in Figure 10d. As shown in Figure 10d, the FCBC, ZCBC, and LCBC successfully loaded metals, and the four adsorbents successfully adsorbed phosphorus. These are consistent with the results of FTIR. The distinguished peaks of La 3d before and after phosphate adsorption are reported in Figure 10f. The representative peaks of La $3d_{5/2}$ for La-BC were centered at 834.7 and 837.8 eV, while La $3d_{3/2}$ peaks were found at 851.6 and 854.7 eV. After adsorption, the double peaks of La $3d_{5/2}$ shift to 835.4 and 838.3 eV, and the peak positions of La $3d_{3/2}$ were at 852.3 and 855.4 eV. There was clear evidence of the binding energies of $3d_{5/2}$ and $3d_{3/2}$ shifting to higher values. This phenomenon suggested the possible electron transfer in the La 3d valence band and the formation of La−O−P inner-sphere complexation.[32,33,35]

The adsorption performance is primarily influenced by the structure and characteristics of the adsorbent. According to Jia et al.[31] and Elkhlifi et al.,[43] the adsorption capacity of

https://doi.org/10.1021/acsomega.3c00788
ACS Omega 2023, 8, 24853−24864

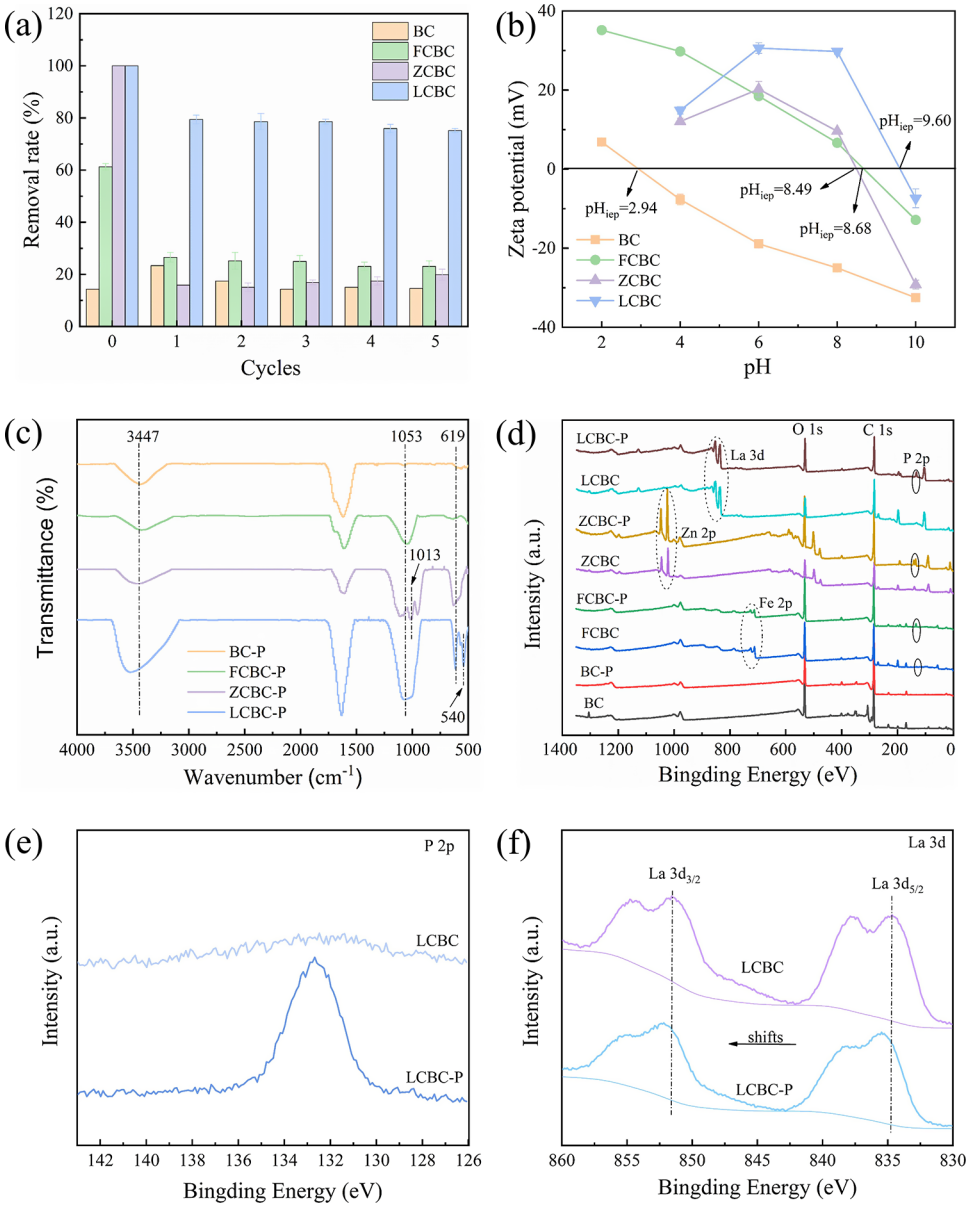

Figure 10. (a) Recycling performance of four adsorbents, (b) zeta potential changes of four adsorbents under different pH conditions, (c) FTIR spectra of BC-P, FCBC-P, ZCBC-P, and LCBC-P, (d) XPS spectra of wide scan before and after adsorption of BC, FCBC, ZCBC, and LCBC, and XPS spectra of (e) P 2p and (f) La 3d for LCBC and LCBC-P.

adsorbents can reach 148.11 and 312.55 mg/g, respectively, when the structure of lanthanum modified adsorbents contains only lanthanum hydroxide crystals. Similarly, Li et al.[38] found that when the structure of lanthanum modified adsorbent contained only lanthanum oxide hydrate crystals, the adsorption capacity of the adsorbent could reach 148.31 mg/g. However, in the present study, the maximum single-layer adsorption capacity of LCBC is up to 666.67 mg/g with both lanthanum hydroxide and hydrated lanthanum oxide crystal forms (Table 3). In summary, we conclude that the lanthanum hydroxide and hydrated lanthanum oxide crystal work synergistically to give the LCBC prepared in this study excellent adsorption capacity.

From the above analysis, we can infer that electrostatic attraction and complexation mechanisms are the two mechanisms by which LCBC binds phosphorus. Electrostatic adsorption is the protonation of the OH groups above La and the biochar to H+, which absorbs negatively charged monohydrogen phosphate and dihydrogen phosphate ions. P═O on the phosphoric acid group has strong polarity, which can induce the break of the OH bond on the carboxyl group and transfer the hydroxyl group to phosphorus. C═O is also highly polar, allowing it to form a σ bond with the remaining lone electron. The oxygen on the phosphate group and the oxygen on the carboxyl group both now possess an extra lone electron, which causes a complexation reaction to occur between the two substances. The mechanism diagram is shown in Figure 11:

4. CONCLUSIONS

In this study, three adsorbents of FCBC, ZCBC and LCBC were successfully prepared by metal chloride modification of waste tobacco sticks. Skeletal-shaped micron-sized particles make up three adsorbents. By comparing the adsorption

https://doi.org/10.1021/acsomega.3c00788
ACS Omega 2023, 8, 24853−24864

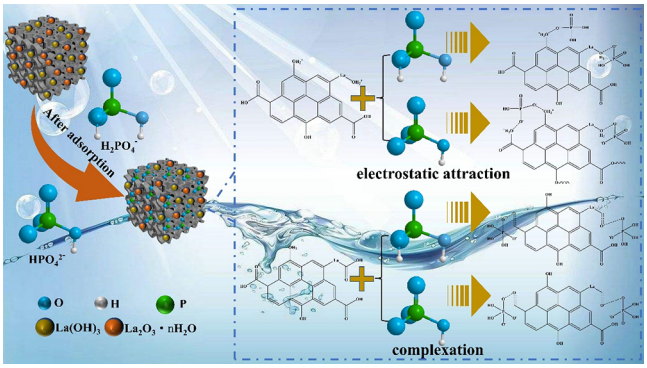

Figure 11. Schematic illustration of the phosphate adsorption on LCBC.

capacity of different adsorbents, the Langmuir isothermal adsorption curve and pseudo-second-order kinetic model were found to adequately describe the phosphate adsorption process of BC, FCBC, ZCBC, and LCBC, and the adsorption behavior was identified as monolayer chemisorption. LCBC has a single molecule adsorption capacity that is approximately 30 times greater than that of BC (22.12 mg g^{-1}) at a maximum of 666.67 mg g^{-1}. The phosphorus adsorption process of the four adsorbents can be divided into three stages according to the model fitting of the intra-particle diffusion. The fact that the second stage does not pass through the origin suggests that additional adsorption stages are controlling the adsorption process and that intra-particle diffusion is not the only rate-limiting step. Zeta potential, FTIR, and XPS results demonstrate that complexation and electrostatic attraction are the primary mechanisms of phosphate adsorption by LCBC. To further absorb phosphorus in the water environment, the positive charge groups and carboxyl groups on the surface of biochar will engage in electrostatic adsorption and complexation reactions with phosphorus. It is found that the metal in LCBC to be in the form of $La(OH)_3$ and hydrated lanthanum oxides. These two types of crystal coexist in LCBC, giving it a high adsorption capacity. After five cycles of recycling in the regeneration cycle experiment, LCBC's phosphorus removal rate was still 75.1%. The result is expected to provide a prospect method for designing and preparing an adsorbent with high adsorption for phosphate removal.

AUTHOR INFORMATION

Corresponding Authors

Bingbing Zhang − *Department of Resources and Environmental, College of Resources and Environmental Engineering, Guizhou University, Guiyang 550025, China; National Engineering Research Center for Compounding and Modification of Polymer Materials, Guiyang 550014, China*; Email: bingbzhang59@163.com

Guomin Xu − *Department of Polymer Material and Engineering, College of Materials and Metallurgy, Guizhou University, Guiyang 550025, China; National Engineering Research Center for Compounding and Modification of Polymer Materials, Guiyang 550014, China*; Email: 1191117410@qq.com, 410034801@qq.com

Authors

Sainan Xia − *Department of Polymer Material and Engineering, College of Materials and Metallurgy, Guizhou University, Guiyang 550025, China*; orcid.org/0000-0002-5155-4148

Shengrong Liang − *Department of Polymer Material and Engineering, College of Materials and Metallurgy, Guizhou University, Guiyang 550025, China*

Yixue Qin − *Department of Polymer Material and Engineering, College of Materials and Metallurgy, Guizhou University, Guiyang 550025, China*

Weijie Chen − *National Engineering Research Center for Compounding and Modification of Polymer Materials, Guiyang 550014, China*

Bin Xue − *National Engineering Research Center for Compounding and Modification of Polymer Materials, Guiyang 550014, China*

Complete contact information is available at: https://pubs.acs.org/10.1021/acsomega.3c00788

Notes

The authors declare no competing financial interest.

ACKNOWLEDGMENTS

This work was financially supported by Fund of Guizhou Province [2020]1Y183, Science and Technology Support Program of Guizhou Province [2020]4Y025, Guizhou Science and Technology Joint Service Enterprise 2021 [9], Science and Technology Support Program of Guizhou Province [2022] General 219.

REFERENCES

(1) Peng, Y.; He, S.; Wu, F. Biochemical processes mediated by iron-based materials in water treatement: Enhancing nitrogen and phosphorus removal in low C/N ratio wastewater. *Sci. Total Environ.* **2021**, *775*, No. 145137.

(2) Yuan, J.; Zhu, Y.; Wang, J.; Liu, Z.; He, M.; Zhang, T.; Li, P.; Qiu, F. Facile modification of biochar derived from agricultural straw waste with effective adsorption and removal of phosphorus from domestic sewage. *J. Inorg. Organomet. Polym. Mater.* **2021**, *31*, 3867−3879.

(3) Ajmal, Z.; Muhmood, A.; Usman, M.; Kizito, S.; Lu, J.; Dong, R.; Wu, S. Phosphate removal from aqueous solution using iron oxides: Adsorption, desorption and regeneration characteristics. *J. Colloid Interface Sci.* **2018**, *528*, 145−155.

(4) Yang, F.; Zhang, C.; Rong, H.; Cao, Y. Research progress and application prospect of anaerobic biological phosphorus removal. *Appl. Microbiol. Biotechnol.* **2019**, *103*, 2133−2139.

(5) Eghombi, E.; Kim, H.; Choi, Y.-H.; Baek, M.-H.; Nadagouda, M. N.; Park, P.-K.; Chae, S. Efficient Phosphorus Recovery from Municipal Wastewater Using Enhanced Biological Phosphorus Removal in an Anaerobic/Anoxic/Aerobic Membrane Bioreactor and Magnesium-Based Pellets. *Membranes* **2022**, *12*, 210.

(6) O'Neal, J. A.; Boyer, T. H. Phosphorus recovery from urine and anaerobic digester filtrate: Comparison of adsorption−precipitation with direct precipitation. *Environ. Sci.: Water Res. Technol.* **2015**, *1*, 481−492.

(7) Lv, N.; Li, X.; Qi, X.; Ren, Y. Calcium-modified granular attapulgite removed phosphorus from synthetic wastewater containing low-strength phosphorus. *Chemosphere* **2022**, *296*, No. 133898.

(8) Gao, Y.; Xie, Y. W.; Zhang, Q.; Wang, A. L.; Yu, Y. X.; Yang, L. Y. Intensified nitrate and phosphorus removal in an electrolysis-integrated horizontal subsurface-flow constructed wetland. *Water Res.* **2017**, *108*, 39−45.

(9) Gao, Y.; Zhang, W.; Gao, B.; Jia, W.; Miao, A.; Xiao, L.; Yang, L. Highly efficient removal of nitrogen and phosphorus in an electrolysis-integrated horizontal subsurface-flow constructed wetland amended with biochar. *Water Res.* **2018**, *139*, 301−310.

(10) Xu, C.; Feng, Y.; Li, H.; Yang, Y.; Jiang, S.; Wu, R.; Ma, R.; Xue, Z. Adsorption of phosphorus from eutrophic seawater using microbial modified attapulgite-cleaner production, remove behavior, mechanism and cost-benefit analysis. *Chem. Eng. J.* **2023**, *458*, No. 141404.
(11) Wang, J.; Zhang, G.; Qiao, S.; Zhou, J. Magnetic Fe^0/iron oxide-coated diatomite as a highly efficient adsorbent for recovering phosphorus from water. *Chem. Eng. J.* **2021**, *412*, No. 128696.
(12) Huang, P.; Liang, Z.; Zhao, Z.; Cui, F. Synthesis of hydrotalcite-like compounds with drinking water treatment residuals for phosphorus recovery from wastewater. *J. Cleaner Prod.* **2021**, *301*, No. 126976.
(13) Lin, L.; Li, Z.; Song, X.; Jiao, Y.; Zhou, C. Preparation of chitosan/lanthanum hydroxide composite aerogel beads for higher phosphorus adsorption. *Mater. Lett.* **2018**, *218*, 201−204.
(14) Ahmad, A.; Rafatullah, M.; Sulaiman, O.; Ibrahim, M. H.; Chii, Y. Y.; Siddique, B. M. Removal of Cu (II) and Pb (II) ions from aqueous solutions by adsorption on sawdust of meranti wood. *Desalination* **2009**, *247*, 636−646.
(15) Wu, L.; Zhang, S.; Wang, J.; Ding, X. Phosphorus retention using iron (II/III) modified biochar in saline-alkaline soils: Adsorption, column and field tests. *Environ. Pollut.* **2020**, *261*, No. 114223.
(16) Feng, Y.; Luo, Y.; He, Q.; Zhao, D.; Zhang, K.; Shen, S.; Wang, F. Performance and mechanism of a biochar-based Ca-La composite for the adsorption of phosphate from water. *J. Environ. Chem. Eng.* **2021**, *9*, No. 105267.
(17) Zhang, T.; Xu, H.; Li, H.; He, X.; Shi, Y.; Kruse, A. Microwave digestion-assisted HFO/biochar adsorption to recover phosphorus from swine manure. *Sci. Total Environ.* **2018**, *621*, 1512−1526.
(18) Wang, H.; Xiao, K.; Yang, J.; Yu, Z.; Yu, W.; Xu, Q.; Wu, Q.; Liang, S.; Hu, J.; Hou, H.; Liu, B. Phosphorus recovery from the liquid phase of anaerobic digestate using biochar derived from iron−rich sludge: A potential phosphorus fertilizer. *Water Res.* **2020**, *174*, No. 115629.
(19) Li, B.; Jing, F.; Hu, Z.; Liu, Y.; Xiao, B.; Guo, D. Simultaneous recovery of nitrogen and phosphorus from biogas slurry by Fe-modified biochar. *J. Saudi Chem. Soc.* **2021**, *25*, No. 101213.
(20) Koh, K. Y.; Zhang, S.; Paul Chen, J. Hydrothermally synthesized lanthanum carbonate nanorod for adsorption of phosphorus: Material synthesis and optimization, and demonstration of excellent performance. *Chem. Eng. J.* **2020**, *380*, No. 122153.
(21) Deng, Y.; Li, M.; Zhang, Z.; Liu, Q.; Jiang, K.; Tian, J.; Zhang, Y.; Ni, F. Comparative study on characteristics and mechanism of phosphate adsorption on Mg/Al modified biochar. *J. Environ. Chem. Eng.* **2021**, *9*, No. 105079.
(22) Wu, D.; Zhan, Y.; Lin, J.; Zhang, Z.; Xie, B. Contrasting effect of lanthanum hydroxide and lanthanum carbonate treatments on phosphorus mobilization in sediment. *Chem. Eng. J.* **2022**, *427*, No. 132021.
(23) Huang, Y.; He, Y.; Zhang, H.; Wang, H.; Li, W.; Li, Y.; Xu, J.; Wang, B.; Hu, G. Selective adsorption behavior and mechanism of phosphate in water by different lanthanum modified biochar. *J. Environ. Chem. Eng.* **2022**, *10*, No. 107476.
(24) Shi, W.; Fu, Y.; Jiang, W.; Ye, Y.; Kang, J.; Liu, D.; Ren, Y.; Li, D.; Luo, C.; Xu, Z. Enhanced phosphate removal by zeolite loaded with Mg−Al−La ternary (hydr)oxides from aqueous solutions: Performance and mechanism. *Chem. Eng. J.* **2019**, *357*, 33−44.
(25) Li, A.; Deng, H.; Wu, Y.; Ye, C.; Jiang, Y. Strong adsorption of phosphorus by ZnAl-LDO-activated banana biochar: An analysis of adsorption efficiency, thermodynamics, and internal mechanisms. *ACS Omega* **2021**, *6*, 7402−7412.
(26) Mitrogiannis, D.; Psychoyou, M.; Baziotis, I.; Inglezakis, V. J.; Koukouzas, N.; Tsoukalas, N.; Palles, D.; Kamitsos, E.; Oikonomou, G.; Markou, G. Removal of phosphate from aqueous solutions by adsorption onto Ca $(OH)_2$ treated natural clinoptilolite. *Chem. Eng. J.* **2017**, *320*, 510−522.
(27) Yang, Q.; Wang, X.; Luo, W.; Sun, J.; Xu, Q.; Chen, F.; Zhao, J.; Wang, S.; Yao, F.; Wang, D.; Li, X.; Zeng, G. Effectiveness and mechanisms of phosphate adsorption on iron-modified biochars derived from waste activated sludge. *Bioresour. Technol.* **2018**, *247*, 537−544.
(28) Yu, H.; Zhang, T.; Jing, Z.; Xu, J.; Qiu, F.; Yang, D.; Yu, L. In situ fabrication of dynamic nano zero-valent iron/activated carbon nanotubes membranes for tellurium separation. *Chem. Eng. Sci.* **2019**, *205*, 278−286.
(29) Zhu, Y.; Rong, J.; Mao, K.; Yang, D.; Zhang, T.; Qiu, F.; Pan, J. Fe_3O_4@chitosan-bound boric acid composite as pH-responsive reusable adsorbent for selective recognition and capture of cis-diol-containing shikimic acid. *Appl. Organomet. Chem.* **2020**, *34*, No. e5415.
(30) Liu, H.; Li, P.; Zhang, T.; Zhu, Y.; Qiu, F. Fabrication of recyclable magnetic double-base aerogel with waste bioresource bagasse as the source of fiber for the enhanced removal of chromium ions from aqueous solution. *Food Bioprod. Process.* **2020**, *119*, 257−267.
(31) Jia, Z.; Zeng, W.; Xu, H.; Li, S.; Peng, Y. Adsorption removal and reuse of phosphate from wastewater using a novel adsorbent of lanthanum-modified platanus biochar. *Process Saf. Environ. Prot.* **2020**, *140*, 221−232.
(32) Tang, Q.; Shi, C.; Shi, W.; Huang, X.; Ye, Y.; Jiang, W.; Kang, J.; Liu, D.; Ren, Y.; Li, D. Preferable phosphate removal by nano-La (III) hydroxides modified mesoporous rice husk biochars: Role of the host pore structure and point of zero charge. *Sci. Total Environ.* **2019**, *662*, 511−520.
(33) Xu, Q.; Chen, Z.; Wu, Z.; Xu, F.; Yang, D.; He, Q.; Li, G.; Chen, Y. Novel lanthanum doped biochars derived from lignocellulosic wastes for efficient phosphate removal and regeneration. *Bioresour. Technol.* **2019**, *289*, No. 121600.
(34) Yan, L.-G.; Yang, K.; Shan, R.-R.; Yan, T.; Wei, J.; Yu, S.-J.; Yu, H.-Q.; Du, B. Kinetic, isotherm and thermodynamic investigations of phosphate adsorption onto core−shell Fe_3O_4@LDHs composites with easy magnetic separation assistance. *J. Colloid Interface Sci.* **2015**, *448*, 508−516.
(35) Li, J.; Li, B.; Huang, H.; Zhao, N.; Zhang, M.; Cao, L. Investigation into lanthanum-coated biochar obtained from urban dewatered sewage sludge for enhanced phosphate adsorption. *Sci. Total Environ.* **2020**, *714*, No. 136839.
(36) Wang, Z.; Shen, D.; Shen, F.; Li, T. Phosphate adsorption on lanthanum loaded biochar. *Chemosphere* **2016**, *150*, 1−7.
(37) Nakarmi, A.; Bourdo, S. E.; Ruhl, L.; Kanel, S.; Nadagouda, M.; Kumar Alla, P.; Pavel, I.; Viswanathan, T. Benign zinc oxide betaine-modified biochar nanocomposites for phosphate removal from aqueous solutions. *J. Environ. Manage.* **2020**, *272*, No. 111048.
(38) Li, S.; Zeng, W.; Ren, Z.; Jia, Z.; Wu, G.; Peng, Y. Performance difference of hydrated phosphorophilic metal oxides in modifying diatomite and recovering phosphorus from wastewater. *Colloids Surf., A* **2021**, *623*, No. 126763.
(39) Wang, Z.; Nie, E.; Li, J.; Yang, M.; Zhao, Y.; Luo, X.; Zheng, Z. Equilibrium and kinetics of adsorption of phosphate onto iron-doped activated carbon. *Environ. Sci. Pollut. Res.* **2012**, *19*, 2908−2917.
(40) Yao, Y.; Gao, B.; Inyang, M.; Zimmerman, A. R.; Cao, X.; Pullammanappallil, P.; Yang, L. Removal of phosphate from aqueous solution by biochar derived from anaerobically digested sugar beet tailings. *J. Hazard. Mater.* **2011**, *190*, 501−507.
(41) Deng, W.; Zhang, D.; Zheng, X.; Ye, X.; Niu, X.; Lin, Z.; Fu, M.; Zhou, S. Adsorption recovery of phosphate from waste streams by Ca/Mg-biochar synthesis from marble waste, calcium-rich sepiolite and bagasse. *J. Cleaner Prod.* **2021**, *288*, No. 125638.
(42) Liao, T.; Li, T.; Su, X.; Yu, X.; Song, H.; Zhu, Y.; Zhang, Y. $La(OH)_3$-modified magnetic pineapple biochar as novel adsorbents for efficient phosphate removal. *Bioresour. Technol.* **2018**, *263*, 207−213.
(43) Elkhlifi, Z.; Sellaoui, L.; Zhao, M.; Ifthikar, J.; Jawad, A.; Shahib, I. I.; Sijilmassi, B.; Lahori, A. H.; Selvasembian, R.; Meili, L.; Gendy, E. A.; Chen, Z. Lanthanum hydroxide engineered sewage sludge biochar for efficient phosphate elimination: Mechanism interpretation using physical modelling. *Sci. Total Environ.* **2022**, *803*, No. 149888.

https://doi.org/10.1021/acsomega.3c00788
ACS Omega 2023, 8, 24853−24864

(44) Nobaharan, K.; Bagheri Novair, S.; Asgari Lajayer, B.; van Hullebusch, E. Phosphorus removal from wastewater: The potential use of biochar and the key controlling factors. *Water* **2021**, *13*, 517.
(45) Jung, K.-W.; Hwang, M.-J.; Ahn, K.-H.; Ok, Y.-S. Kinetic study on phosphate removal from aqueous solution by biochar derived from peanut shell as renewable adsorptive media. *Int. J. Environ. Sci. Technol.* **2015**, *12*, 3363−3372.
(46) Fu, H.; Yang, Y.; Zhu, R.; Liu, J.; Usman, M.; Chen, Q.; He, H. Superior adsorption of phosphate by ferrihydrite-coated and lanthanum-decorated magnetite. *J. Colloid Interface Sci.* **2018**, *530*, 704−713.

https://doi.org/10.1021/acsomega.3c00788
ACS Omega 2023, 8, 24853−24864